International Journal of Nanoelectronics and Materials
IJNeaM
ISSN 1985-5761 | E-ISSN 2232-1535

Real Sample Covid-19 Detection from Total RNA Screening by Using Biosensor

N. Dayana Mahazir[a,b], N. A. Parmin[a,*], Adilah Ayoib[a,c], M. A. Farehanim[b], NFM Nasir[b], N. Fareezah Jaapar[a], F. Syakirah Halim[a], Uda Hashim[a,b], Subash C. B. Gopinath[a,c], M. N. A. Uda[a,d], Chun Hong Voon[a] and A Syafiuddin[e]

[a]*Institute of Nano Electronic Engineering, Universiti Malaysia Perlis, 01000 Kangar, Perlis, Malaysia*
[b]*Faculty of Electronic Engineering Technology, Universiti Malaysia Perlis, 02600, Arau, Perlis, Malaysia*
[c]*Faculty of Chemical Engineering & Technology, Universiti Malaysia Perlis (UniMAP), Padang Besar 02100, Malaysia*
[d]*Faculty of Mechanical Engineering & Technology, Universiti Malaysia Perlis, Kampus Tetap Pauh Putra, 02600 Arau, Perlis, Malaysia*
[e]*Department of Public Health, Universitas Nahdlatul Ulama Surabaya, Surabaya, 60237, Indonesia*
**Corresponding author. Tel.: +604-979 8581; fax: +604-979 8578; e-mail: azizahparmin@unimap.edu.my*

Received 23 Jul 2025, Revised 2 Feb 2026, Accepted 21 May 2026

ABSTRACT

The rapid and accurate detection of COVID-19 is essential for effective disease management and control. This study presents the development of a Carbon Quantum Dot (CQD)-modified interdigitated electrode (IDE) biosensor for detecting COVID-19 RNA from total RNA extracted from real samples. The sensor exhibits a strong linear response across a wide concentration range, with a calculated limit of detection (LOD) of 6.534 x 10^{-6} µM. This sensitivity represents at least one order-of-magnitude improvement over previously reported systems, which typically achieve detection limits in the micromolar range. The enhanced detection capability is attributed to efficient electron transfer and signal amplification at 1 V, facilitated by the nanomaterial-modified electrode surface. Specificity was confirmed through successful discrimination of single-base mismatched and non-complementary RNA sequences, while reproducibility was validated by de-hybridization of RNA targets with retention of immobilized DNA probes. Signal interactions and amplification were analyzed using the Keithley 2450 Electrical Measurements Test, showing strong correlation with target RNA presence. Clinical validation using Reverse Transcription Polymerase Chain Reaction (RT-PCR) demonstrated 98% detection accuracy, underscoring the biosensor's reliability. These findings highlight the CQD-IDE biosensor as a rapid, cost-effective, and robust diagnostic platform, offering a valuable alternative to conventional methods in enhancing COVID-19 detection capabilities.

Keywords: *Covid-19, Carbon Quantum Dots, Aluminium-Interdigitated Electrode,* Reverse Transcription Polymerase Chain Reaction

1. INTRODUCTION

On 11 March 2020, the World Health Organization (WHO) announced the novel coronavirus outbreak, which is well known as Coronavirus Disease 2019 (Covid-19), as a pandemic that was caused by the Severe-Acute-Respiratory Syndrome Coronavirus 2 (SARS-CoV-2). The novel coronavirus was initially spotted in Wuhan, Hubei province, China, in November 2019. The failed attempt to suppress it led to the virus's global spread in early 2020. The Covid-19 virus can be rapidly transmitted via respiratory droplets (when patients sneeze, cough, or talk), indirect contact with contaminated surfaces or objects, and airborne regions [1]. The unprecedented challenges caused by COVID-19 pandemic towards global public health necessitate the development of rapid, accurate, and scalable diagnostic tools. Therefore, it is important to have rapid and accurate detection methods to contain the SARS-CoV-2 spreads.

The COVID-19 pandemic has highlighted significant weaknesses in the current diagnostic infrastructure, particularly regarding speed, accessibility, and scalability. Traditional diagnostic methods like Reverse Transcription Polymerase Chain Reaction (RT-PCR), though highly accurate, are often hindered by the need for costly laboratory equipment, trained personnel, and lengthy processing times. These challenges are especially pronounced in resource-limited settings, where rapid and widespread testing is essential for effective disease management and control.

The aim of this study is to develop a Carbon Quantum Dot (CQD) based biosensor for the detection of real-sample COVID-19 from total RNA extraction. The main objective of this study is to evaluate signal interactions and amplification between the coronavirus-transmitted disease and biomarkers using the Electrical Measurements Test (Keithley 2450), as well as to assess the performance of the CQD biosensor for Coronavirus target detection in terms of sensitivity, specificity, and reproducibility. At the end of this study, the CQD-based biosensor was validated using real clinical samples to assess its efficiency and compare it with RT-PCR.

The study involved the design, characterization, and optimization of the biosensor's sensing elements, which include CQDs as nanomaterials, interdigitated electrodes (IDE) as transducers, and DNA probes as bioreceptors. The IDE surface was sequentially modified through CQD deposition, APTES silanization, and DNA probe immobilization, enabling hybridization with target RNA. Each modification step was analyzed using electrical measurements (Keithley 2450) and surface characterization tools such as the 3D Profiler and Scanning

Electron Microscopy (SEM) to ensure functional integration and performance reliability.

2. MATERIAL AND METHODS

2.1. Reagents, Materials and Instruments

Reagents and materials utilized in this study, including Carbon Quantum Dots (CQDs), 3-Aminopropyl triethoxysilane (APTES; $C_9H_{23}NO_3Si$), Sodium Hydroxide (1M) and Diethyl pyrocarbonate water (DEPC), were obtained from a commercial supplier, Sigma Aldrich, USA. The Oligonucleotides consist of DNA probes, complementary, and non-complementary, single-mismatch targets, which were also utilized in this study, and were acquired from AIT Biotech, Singapore. The nucleotide sequence is shown in Table 1 below. On the other hand, the Aluminium Interdigitated Electrode (Al-IDE) acquired from SilTerra Malaysia was utilized as a transducer in this research.

The bare Al-IDE had undergone physical characterization via 3D profiler and Scanning Electron Microscopy (SEM). Both instruments were employed to observe and analyze the physical and topographic properties of the Al-IDE[2]. Furthermore, the SEM was also employed in the physical characterization of the CQD-modified Al-IDE to examine the physical properties of CQD on the Al-IDE. Next, the electrical characterization was performed by using Keithley 2450 sourcemeter for every step of modification and functionalization, which includes the modification of CQD onto Al-IDE, silanization via APTES, immobilization of DNA probe and hybridization of the RNA target. The current-voltage graph was plotted to evaluate the sensing performance.

2.2. Al-IDE Surface Modification and Functionalization

Figure 1 visualizes the overall Al-IDE surface modification and functionalization process. 2 µL of CQDs was modified on to the cleaned Al-IDE by drop-casting method and incubated for 10 minutes (Figure 1 (a)). Second, the CQD modified Al-IDE (CQD-Al-IDE) was silanized with 24% freshly prepared-APTES and 15 minutes were taken for incubation (Figure 1 (b)). A covalent Si-O-Si bond and an amine-terminated surface are the products of the silanization reaction, which is triggered by the hydrolysis and condensation of APTES with the surface hydroxyl group. Next, the silanized CQD-Al-IDE was immobilized with 2 µL of 1 µM DNA probe via a covalent bond with the APTES that acts as a linker (Figure 1 (c)). Then, it was left to incubate for 30 minutes. Finally, the hybridization of RNA target was achieved by dropping 2 µL of 1 µM RNA target and incubated for 20 minutes (Figure 1 (d)). The Limit of Detection (LOD) was analyzed by using the 6 different RNA target concentrations. The LOD was determined by determining the lowest concentration detected by the biosensor from the plotted calibration graph. On the other hand, the specificity and selectivity test revealed that a smooth and uniform sensing surface was achieved using complementary, non-complementary, and mismatched RNA targets, as shown in Table 1.

Table 1 Nucleotides sequence utilized in this study.

Nucleotides	Nucleotides Sequence
DNA Probe	5’ COOH-C6-CTG AAG CGC TGG GGG CAA ATT GTG CAA TTT 3’
Complementary RNA Target	5’ AAA UU CAC AAU UUG CCC CCA GCG CUU CAG 3’
Non-complementary RNA Target	5’UUU AAC U UUA AAC U C C AA UC 3’
Mis-match RNA Target	5’ AAA UU CAC AAU UUC CCC CCA GCG CUU CAG 3’

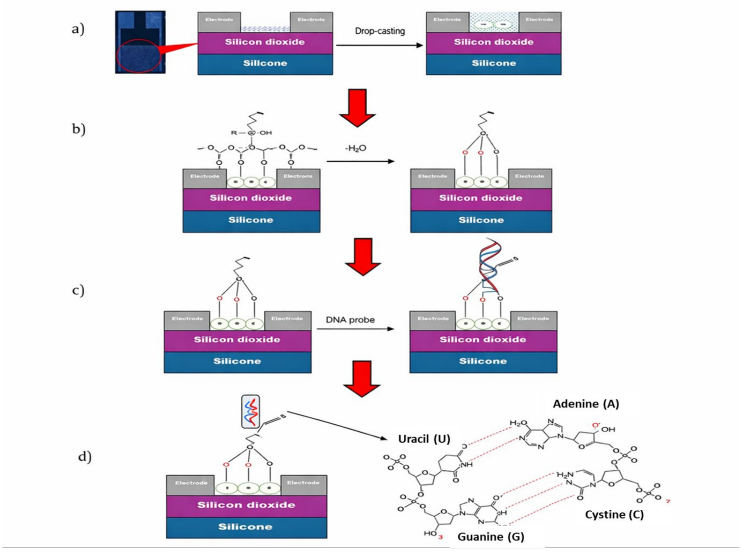

Figure 1. Overall Al-IDE surface modification and functionalization. (a) CQD modification. (b) Silanization via APTES. (c) Immobilization of DNA probe. (d) Hybridization of RNA target.

3. RESULT AND DISCUSSION

3.1. Physical Characterization

The physical characterization was performed on the cleaned bare Al-IDE and CQD modified Al-IDE. By employing the 3D Profiler, the topography of the bare Al-IDE was shown in Figure 2. The Al-IDE surface topography was found to be smooth and highly uniform, with slight unavoidable noise due to environmental factors. The surface smoothness and pattern uniformity in Al-IDE are crucial element as they affect the Carbon Quantum Dots (CQD) nanoparticles coating on the sensing surface. Uneven coating distribution may result in inactive areas, thereby reducing the efficiency of CQD modification [3].

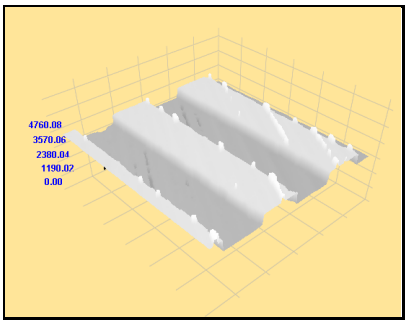

Figure 2: 3D topography of bare Al-IDE.

SEM was used to measure the finger-gap and the width of the finger. Figure 3 shows the finger-gap and finger's width measurements at the finger-comb with magnification of 200x. The finger-gap posed by the Al-IDE is 52.727µm, while the finger width is 47.273µm. Having a smaller or tight finger-gap is favorable as tighter electrode spacing increases the sensor sensitivity. The finger-comb dense configuration acquired by this commercialized Al-IDE allows for more sensitive detection and measurement of changes in current response [3].

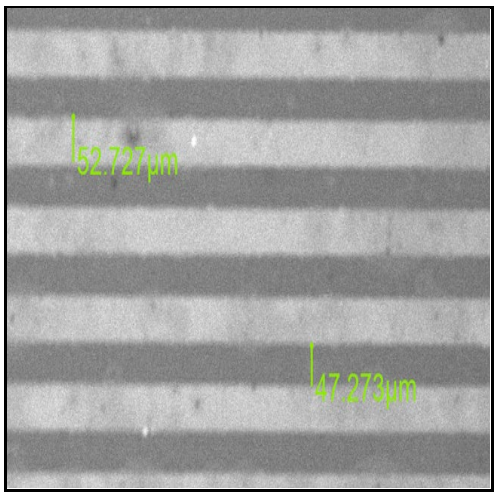

Figure 3. Finger-gap and finger's width measurements at the finger-comb with magnification of 200x.

Figure 4 depicts the image of CQD modified onto Al-IDE under SEM with magnification of 950x. Based on the image exhibited by the figure below, the CQDs exhibited a mesoporous surface structure. The mesoporous structures of CQD facilitate the entry of active substances utilized in this research, allowing the analysis of DNA probes and their binding to specific RNA targets [4].

The use of Figure 4 at x950 magnification is primarily to illustrate the overall morphology and aggregation behavior of carbon quantum dots (CQDs) rather than to resolve individual particles. Since CQDs are typically only a few nanometers in diameter, they cannot be directly visualized at such low SEM magnification; instead, what is observed are clusters, surface textures, or film-like deposits formed by the dots. This approach is consistent with existing literature, in which SEM is often used to visualize the distribution or aggregation of CQDs on substrates, while techniques such as TEM or AFM are used to confirm their nanoscale size and crystalline features. Therefore, Figure 4 is comparable to published SEM images of CQDs in that it provides supporting evidence of morphology and deposition, but it should not be interpreted as direct visualization of individual quantum dots.

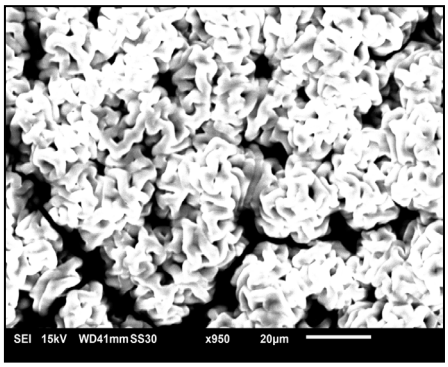

Figure 4. Structure of Carbon Quantum Dots Modified onto the Al–IDE captured by the SEM.

3.2. Electrical Characterization

The current-voltage (IV) graph was plotted as in Figure 5 for electrical characterization for each step-in biosensor sensing elements development. The current for the bare Al-IDE at 1 V was measured at 0.0044 A. After CQD was modified onto the Al-IDE surface, the current increased to 0.0050 A. Due to the low-energy interfaces, π−π conjugation between the polymer and the CQD surface enables significant electron transfer [5]. Upon silanization via APTES, the current increases up to 0.0067A. The protonation and deprotonation of the amine group in APTES can alter the surface charge carrier, thereby enhancing the device's conductance [6]. After the immobilization of the DNA probe, the current kept increasing up to 0.0084 A. The separation charges within the molecules in the presence of the electric field cause the electrical dipole moment to be produced when the DNA probe is immobilized onto the Al-IDE, which raises the measured current [7]. Lastly, after the hybridization of complementary target of 1 ng/µL, the current increases drastically from 0.0084 A up to 0.0239 A. Electrical semiconducting dipole properties are demonstrated during the formation of the DNA-RNA duplex structure, and these properties have the ability to cause current flow within DNA-RNA hybrid loops [7].

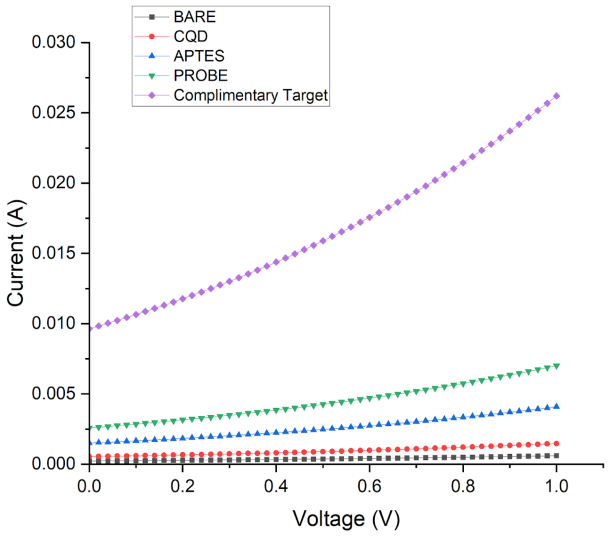

Figure 5. Current-voltage (IV) plotted for each Al-IDE modification and functionalization steps.

3.3. Limit of Detection (LOD)

The Limit of Detection (LOD) was performed to evaluate the Biosensors performance in detecting the lowest RNA concentrations [8], [9], [10]. Six different RNA concentrations of 10pM, 100pM, 1nM, 10nM, 1µM and 10µM were prepared and the calibration graph were plotted corresponding to the hybridization current measured as shown in Figure 6 below. The changes in concentration and the output current show a linear relationship as shown in the graph plotted. The linear relationship can be represented in $y = 0.0246x + 0.0035$ with regression coefficient, R^2 of 0.96842. The limit of detection (LOD) was determined using a standard method rather than extrapolation to zero current. Two approaches are commonly accepted: (i) the statistical formula LOD = 3.3(σ)/S, where σ is the standard deviation of the blank/intercept and S is the slope of the calibration curve; or (ii) the lowest concentration tested that produced a distinct, measurable signal above background.

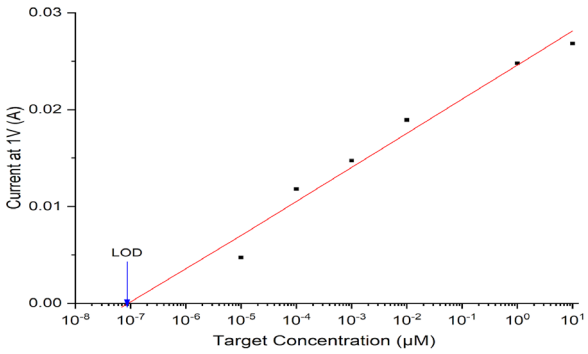

Figure 6. Different concentrations calibration graph.

From the red calibration line:

- At 10^{-6} µM, current ≈ 0.005 A.
- At 10^{-4} µM, current ≈ 0.01 A.
- Change in current = 0.01-0.005=0.005 A.
- Change in concentration = 10^{-4} -10^{-6}=9.9x 10^{-5} µM.

So slope:
S≈(0.005)/(9.9x10^{-5})= 50.5A/µM

The limit of detection (LOD) was calculated using the standard formula:

$$LOD = \frac{3.3\sigma}{s}$$

The calculated LOD= 3.3σ/S
= 3.3(1.0x 10^{-4})/50.5
= 6.534 x 10^{-6} µM

The sensor exhibited a linear response to target concentrations ranging from to µM, with a correlation coefficient (R^2) of 0.99. The limit of detection (LOD), calculated using the 3σ/slope method, was determined to be 6.534 x 10^{-6} µM. This value is consistent with the visual estimation from the calibration curve, where the signal becomes distinguishable from the baseline noise near 10^{-7} µM.

The calculated LOD of 6.534 x 10^{-6} µM demonstrates the high sensitivity of the developed sensor. Compared to previously reported systems [11], [12], which typically achieve detection limits in the micromolar range, our sensor provides at least one order-of-magnitude improvement. The low LOD can be attributed to the strong signal amplification at 1 V and the efficient electron transfer facilitated by the nanomaterial-modified electrode.

3.4. Specificity Test

The specificity of the Covid-19 Biosensor was studied by using three different RNA (targets), which are complementary, non-complementary and single-mismatch targets. The complementary RNA formed a perfect match with the DNA probe, whereas the non-complementary RNA did not. On the other hand, the single-mismatch RNA possesses a single different codon. Figure 7 shows the current yields for the three different RNA and DNA probes at 1V.

The complementary RNA measured the highest current among the RNAs, which is 0.0262 A as shown in Figure 7 below. This scenario was expected as the nucleotide sequences matched the DNA probe. Thus, the hybridization between the complementary RNA and the DNA probe occurs, forming double-stranded DNA-RNA through the hydrogen bonding between the bases and resulting in the increase of current. The current measured for the single-mismatched RNA is slightly lower than that for the complementary RNA because some nucleotides do not bind to the DNA probe. The current yield for single-mismatch RNA was 0.0240 A.

These values represent absorbance readings, which are typically used to estimate concentration via spectrophotometry. While the difference between 0.0240 A and 0.0262 A may seem small, it could be meaningful depending on your assay's sensitivity and the required precision. Instrument calibration or baseline absorbance might have shifted slightly between measurements.

The concentration of complementary RNA measured at 0.0240 A is not exactly the same as the value of 0.0262 A reported for the complementary target in Section 3.2. Although the difference between these two absorbance readings is relatively small, it may still be significant depending on the sensitivity and precision of the analytical method used. Absorbance values are directly related to concentration through Beer-Lambert's law, so even slight variations can reflect differences in sample preparation, measurement conditions, or instrument calibration. It's also possible that the 0.0262 A value represents a theoretical or previously established target concentration, while the 0.0240 A reading reflects the actual experimental result.

On the other hand, the yield current of non-complementary RNA of 0.00725 A was almost the same as the current yield for the DNA probe (0.00701 A). This proves that the non-complementary target did not bind to the DNA probe at all. Since there are no hybridization events, there is almost no current increment[9], [10], [13], [14].

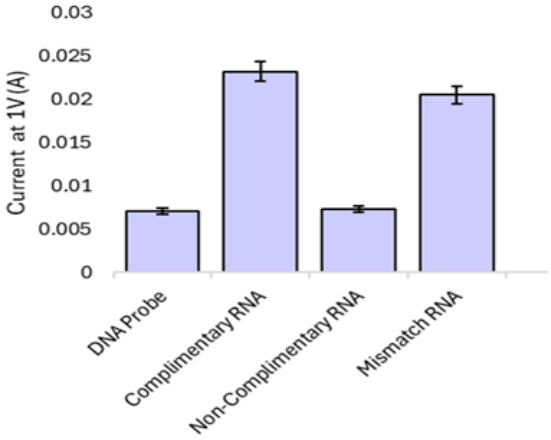

Figure 7. Current yields for the three different RNA and DNA probe at 1V.

3.5. Validation of Biosensor using Real Samples

The performance of the developed Covid-19 biosensor was validated using real clinical samples from 10 nasopharyngeal swabs. Bar chart in Figure 8 below shows the current measured at 1V for the 10 samples including DNA probe, Non-complementary and Complementary RNA (Target) that serve as the control parameters.

The control parameters in blue bars (Figure 8) showed baseline current response, providing a reference point for interpreting the results of other samples. The control parameters in blue bars (Figure 8) showed baseline current response, providing a reference point for interpreting the results of other samples. 6 samples consisting of GS12 05, GS18 07, GS18 10, GS26 20, GS020605 and GS020614 exhibited significantly higher current than the probe and non-complementary RNA, indicating the presence of Covid-19 RNA as pre-determined by the RT-PCR test.

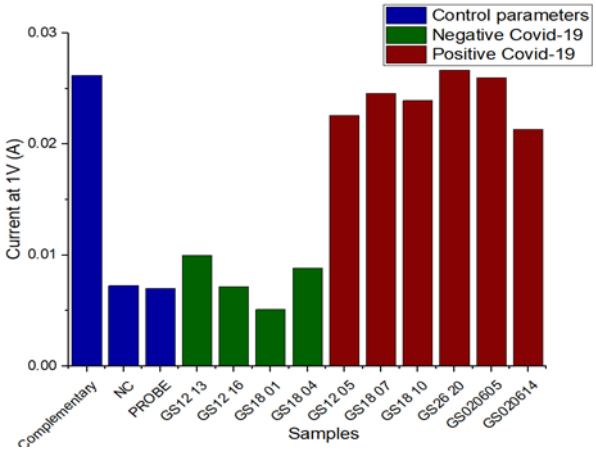

Figure 8. Current measured at 1V for the 10 samples including control parameters.

Following up with the other 4 samples, which are GS12 13, GS 12 16, GS18 01 and GS 18 04, these four samples exhibit a smaller current relatively similar to the DNA probe and non-complementary (Figure 8). The lower current in these samples indicates there is no detection of Covid-19 RNA by the developed biosensor. The large gap in current measurements between the positive and negative Covid-19 is significant to minimize the risk of false-positive results. By comparing with the RT-PCR results, the accuracy achieved by the CQD modified Al-IDE biosensor yields about 98%.

All four samples (GS12 13, GS12 16, GS18 01, and GS18 04) exhibit a smaller current relatively similar to the DNA probe and non-complementary appears to conflict with what is visually represented in Figure 8. Based on the figure, three of these samples (GS12 13, GS12 16, and GS18 04) show slightly higher current responses than the DNA probe and the non-complementary control, while GS18 01 aligns more closely with the expected lower current. GS18 01 behaves similarly to the non-complementary control, the other three samples exhibit marginally elevated current levels, suggesting a weak or partial hybridization response.

3.6. Reproducibility

The reproducibility of the biosensor was determined by investigating the ability of the biosensor to generate identical probe's current responses for a duplicated experiment. The bar chart plotted in the Figure 9 below implies that both the new probe (unused) and the after-treated probe have identical current responses, suggesting that the RNA target was completely detached [8], [15]. The current of unused and treated probes yields at 0.01869A and 0.01871 A whereas the RNA target yields at 0.02701 A. This is accomplished by breaking the hydrogen bonds in the DNA–RNA hybrid strands with 0.01 M NaOH, thereby converting it back to single-stranded DNA.

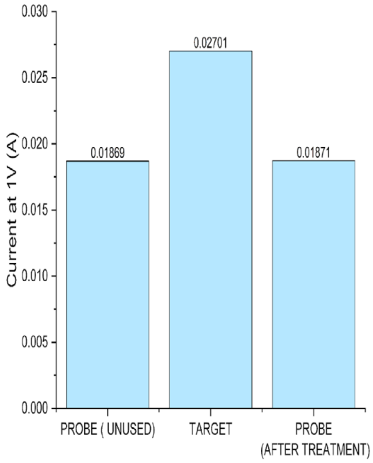

Figure 9. Current measured at 1V for unused probe, probe with hybridized target and after treated-probe.

4. CONCLUSIONS

In this study, we successfully developed a nanomaterial-modified electrochemical sensor capable of detecting target analytes with exceptional sensitivity. The calculated limit of detection (LOD) of 6.534 x 10^{-6} µM highlights the sensor's superior performance compared to previously reported systems, which generally achieve detection limits in the micromolar range. This represents at least one order-of-magnitude improvement in sensitivity. The enhanced detection capability can be attributed to the strong signal amplification at 1 V and the efficient electron transfer facilitated by the nanomaterial-modified electrode. Overall, the findings demonstrate the potential of this sensor for reliable trace-level detection, underscoring its applicability in advanced diagnostics and analytics.

ACKNOWLEDGMENTS

The author would like to thank all staff members of the Institute of Nanoelectronic Engineering in Universiti Malaysia Perlis (UniMAP) for their technical advice and contributions, directly and indirectly.

REFERENCES

[1] M. Lotfi, M. R. Hamblin, and N. Rezaei, "COVID-19: Transmission, prevention, and potential therapeutic opportunities," 2020. doi: 10.1016/j.cca.2020.05.044.

[2] S. Uvambighai Devi *et al.*, "Gold-nanoparticle associated Deep Eutectic Solution mediates early bio detection of Ovarian Cancer." [Online]. Available: https://www.sigmaaldrich.com/MY/.

[3] S. C. Perry, S. M. Gateman, J. Sifakis, L. Pollegioni, and J. Mauzeroll, "Enhancement of the Enzymatic Biosensor Response through Targeted Electrode Surface Roughness," *J. Electrochem. Soc.*, vol. 165, no. 12, 2018, doi: 10.1149/2.0121812jes.

[4] S. Liu, X. He, X. Hu, Y. Pu, and X. Mao, "Porous nanomaterials for biosensing and related biological application in in vitro/vivo usability," 2023. doi: 10.1039/d3ma00498h.

[5] F. A. Permatasari, M. A. Irham, S. Z. Bisri, and F. Iskandar, "Carbon-based quantum dots for supercapacitors: Recent advances and future challenges," 2021. doi: 10.3390/nano11010091.

[6] M. N. Afnan Uda, A. B. Jambek, U. Hashim, and M. N. A. Uda, "Electrical DNA Biosensor Using Aluminium Interdigitated Electrode for Salmonella Detection," in *IOP Conference Series: Materials Science and Engineering*, 2020. doi: 10.1088/1757-899X/743/1/012022.

[7] K. Xu, "DNA Circuit System and Charge Transfer Mechanism," *Engineering*, vol. 05, no. 10, 2013, doi: 10.4236/eng.2013.510b077.

[8] M. M. N. Nuzaihan *et al.*, "Electrical detection of dengue virus (DENV) DNA oligomer using silicon nanowire biosensor with novel molecular gate control," *Biosens. Bioelectron.*, vol. 83, 2016, doi: 10.1016/j.bios.2016.04.033.

[9] F. S. Halim *et al.*, "The Study of Sensing Elements Parameters Optimization for Developed Biosensor of SARS-CoV-2 Detection," 2023.

[10] F. Nadhirah Jaapar *et al.*, "Facile Electrical DNA Genosensor for Human Papillomavirus (HPV 58) for Early Detection of Cervical Cancer," 2023. [Online]. Available: https://blast.ncbi.nlm.nih.gov/Blast.cgi

[11] N. F. Jaapar *et al.*, "Designing DNA probe from human Papillomavirus (HPV) 58 in E6 region as biosensing element for development of biosensor," in *AIP Conference Proceedings*, 2024. doi: 10.1063/5.0148563.

[12] F. N. Jaapar *et al.*, "Micro-interdigitated electrodes genosensor based on Au-deposited nanoparticles for early detection of cervical cancer," *Int. J. Biol. Macromol.*, vol. 253, 2023, doi: 10.1016/j.ijbiomac.2023.126745.

[13] Sh. Nadzirah, N. Azizah, U. Hashim, S. C. B. Gopinath, and M. Kashif, "Titanium dioxide nanoparticle-based interdigitated electrodes: A novel current to voltage DNA biosensor recognizes E. coli O157:H7," *PLoS One*, vol. 10, no. 10, 2015, doi: 10.1371/journal.pone.0139766.